
A computational model for texture analysis in images with a reaction-diffusion based filter

Lefraich Hamid[‡], Houda Fahim[†], Mariam Zirhem[†], Nour Eddine Alaa^{†*},

[‡]Laboratory (MISI), Faculty of Science and Technology, University Hassan first, Settat
26000, Morocco

[†]Laboratory LAMAI, Faculty of Science and Technology, Cadi Ayyad University, Morocco

Email(s): lefraichhamid@gmail.com, houda.fahim@edu.uca.ma,
mariam.zirhem@edu.uca.ac.ma, n.alaa@uca.ac.ma

Abstract. As one of the most important tasks in image processing, texture analysis is related to a class of mathematical models that characterize the spatial variations of an image. In this paper, in order to extract features of interest, we propose a reaction diffusion based model which uses the variational approach. In the first place, we describe the mathematical model, then, aiming to simulate the latter accurately, we suggest an efficient numerical scheme. Thereafter, we compare our method to literature findings. Finally, we conclude our analysis by a number of experimental results showing the robustness and the performance of our algorithm.

Keywords: Reaction-diffusion system, biomedical images, texture analysis

AMS Subject Classification 2010: 34A34, 65L05.

1 Introduction

Texture analysis is a branch of image processing that describes the characteristics of an image by means of its texture features. It is used in many image processing disciplines such as classification, segmentation and synthesis. Texture extraction methods are numerous and are divided into geometrical, statistical, model-based and structural approach. They are widely applied in biomedical applications in order to differentiate normal from abnormal tissues or to identify human organs. Readers interested in this fascinating field can be referred to the book [10]. Before approaching our main contribution, we will provide a brief overview of different methods used in the literature for the texture analysis of biomedical images. For instance, Brady et al. [3] used a statistical method to extract texture and to classify mammography images. Their approach is based on three steps: the first one is the segmentation of the mammogram into three components, then the extraction of a set of features from the image and finally the classification of

*Corresponding author.

Received: 28 November 2020 / Revised: 21 January 2021 / Accepted: 7 February 2021

DOI: 10.22124/jmm.2021.18289.1569

parenchymal pattern. In addition, Freedman et al. [12] proposed a method for automatic classification of mammographic parenchymal patterns, based on the derivation of textons dictionary from the training set. It uses the density of patterns which incorporates representation of space features and detects breast cancer risk.

Furthermore, Sayeed et al. [21] used a new technique known as the triple features trace transform in order to distinguish patients with Alzheimer's disease from normal controls. This method was used to extract features that are invariant to scaling, translation and rotation. After that, Kovalek et al. [15] showed the difference between the brains of schizophrenic and normal control by using 3D texture analysis for measuring the anisotropy in the employed data at finest scale. This technique reveals that the features that distinguish between the two populations are located in the most inferior part of the brain. Moreover, Chabat et al. [5] proposed an automated technique, which is based on a statistical method and was used to differentiate a large variety of obstructive lung diseases in computed tomographic images (CT). This approach allows the extraction of textural information contained within the image and it presents a good result for texture analysis of similar type of images. Aiming to improve the characterization of brain tumor by using three dimensional co-occurrence matrix, Ghoneim et al. [13] compared their approach with 2D and 3D texture analysis and they found that their approach ensures a better separation of different cerebral tumors. Thus, their method can be used as a new tool in disease's control. A standardized technique focused on color correction and texture characteristics analysis was introduced by Neofytou et al. [17] in order to eliminate significant differences of endoscopic images. They used statistical methods to analyze the extracted features.

Besides that, a method was used to extract tumor from magnetic resonance imaging scans of human head [18]. The brain tumor is located through wavelet packet, then the energy minimization resulting from the level set is updated at each iteration of the process and finally the tumor is extracted when the stopping criterion is achieved. A fractal analysis procedure for the processing of visual textures was investigated in the work of Dennis et al. [24]. To calculate the rate of change of a local estimate of the fractal dimension at different scales and orientations the authors used second order spatial statistics. It has been shown that the method is able to test the validity of fractal model for real visual textures. Furthermore, texture information is extracted via a color space model and nonsubsampling contourlet transform. Then, the extracted color and texture information are transformed efficiently into the neutrosophic set domain by the approach proposed by Heshmati et al. [25]. All the aforementioned methods are restricted to quantify anisotropy of textural information presented in biomedical images. Unfortunately, this can't diagnostic certain diseases that require more details on a small scale of the order of millimeters so as to describe a well-suited treatment. To do so, several researches concerning texture analysis have been made by involving variational partial differential equation models. These models aims to decompose a given image u_0 defined on a bounded open domain $\Omega \subset \mathbb{R}^2$ into the sum of two components. The key here is to keep the homogeneous regions with sharp boundaries of u_0 in a part which is called cartoon or geometric component, and to put the repeated patterns of small scale details in a texture part. To separate these components, many researchers used the total variation (TV) of the image so as to obtain the geometrical part and they chose different norms of texture in order to keep it small. Among these works, we mention the model of Rudin et al. [20], which was one of the most popular work in image decomposition. In their problem, the cartoon part belongs to the space of functions of bounded variation $BV(\Omega)$

which is defined as follow

$$BV(\Omega) = \{u \in L^1(\Omega); \int_{\Omega} |Du| < \infty\}, \quad (1)$$

where

$$\int_{\Omega} |Du| = \sup \left\{ \int_{\Omega} u \operatorname{div}(\varphi) / \varphi \in C_0^\infty(\Omega, \mathbb{R}^2), \|\varphi\|_{L^\infty(\Omega)} \leq 1 \right\},$$

is the total variation of u . This space allows for edges or discontinuities along curves. Hence, edges and contours are kept in the geometric component u while details of small scale are still in $u_0 - u$. Their model is given as the following minimization problem

$$\min_{u \in BV(\Omega)} \int_{\Omega} |Du| + \lambda \|u_0 - u\|_{L^2(\Omega)}^2. \quad (2)$$

For the mathematical study of this model, Chambolle et al. [7] gave results of existence and uniqueness. Furthermore, Chambolle [6] proposed also a projection algorithm for the numerical simulation of (2). However, this model fails to separate cartoon from texture components. Aiming to tackle that issue, Meyer [16] suggested to replace the norm L^2 in the problem (2) by a weaker norm which could be more appropriate for modeling textured or oscillatory patterns. Meyer proposed the following minimization problem

$$\min_{u \in BV(\Omega)} \int_{\Omega} |Du| + \lambda \|u_0 - u\|_{G(\Omega)}, \quad (3)$$

where $G(\Omega)$ is the Banach space composed of distributions v that can be written as

$$v = \frac{\partial g_1}{\partial x_1} + \frac{\partial g_2}{\partial x_2} = \operatorname{div}(g), \quad (4)$$

with $g = (g_1, g_2) \in (L^\infty(\Omega))^2$ and $\frac{\partial g_1}{\partial x_1}, \frac{\partial g_2}{\partial x_2}$ are respectively the derivatives of g_1 and g_2 in the distributional sense. The space $G(\Omega)$ is endowed with the following norm:

$$\|v\|_{G(\Omega)} = \inf \{ \|g\|_{L^\infty(\Omega)} / v = \operatorname{div}(g) \}. \quad (5)$$

The difficulty with this minimization problem (3) is that it can't be solved directly due to the norm of G . To deal with Meyer's model, Osher et al. [19] presented a model that uses the H^{-1} norm for oscillatory functions under a total variation minimization framework,

$$\min_{u \in BV(\Omega)} \int_{\Omega} |Du| + \lambda \|u_0 - u\|_{H^{-1}(\Omega)}^2, \quad (6)$$

where $\lambda > 0$ is a weight parameter and the H^{-1} norm is defined as follows:

$$\|\cdot\|_{H^{-1}(\Omega)}^2 = \int_{\Omega} |\nabla \Delta^{-1}(\cdot)|^2 dx,$$

where $(-\Delta^{-1})$ is the inverse Laplacian operator. This problem can be solved by following the formalism of Chambolle [6]. There is another model that replaces the norm L^2 of the fidelity term in (3) by the norm in L^1 space. It is known as TV- L^1 model [23], namely

$$\min_{u \in BV(\Omega)} \int_{\Omega} |Du| + \lambda \|u_0 - u\|_{L^1(\Omega)}. \tag{7}$$

This norm is well suited for cartoon and texture separation since it's more able to preserves geometric features than the L^2 norm and more appropriate for representing textured or oscillatory patterns. The authors applied to their model the implementation of the primal dual algorithm proposed by [8]. A generalization of the models of Rudin et al. [20] and Osher et al. [19] was proposed by Aujol et al. [1]:

$$\min_{u \in BV(\Omega)} \int_{\Omega} |Du| + \lambda \|u_0 - u\|_H(\Omega), \tag{8}$$

where H is a Hilbert space. By an appropriate choice of this space, the authors decomposed the image into geometrical and textural information by using Gabor wavelets. Furthermore, they showed the existence and uniqueness of a solution for their model and they also proposed a modification of Chambolle's projection algorithm to compute their solution. In 2006, Aujol et al. [2] proposed a two-part decomposition of an image into both structure and texture components. Indeed, they proposed a regularization of TV- L^1 model, defined as follows:

$$\min_{(u,v)} \int_{\Omega} |Du| + \frac{1}{2\alpha} \|u_0 - u - v\|_{L^2}^2 + \lambda \|v\|_{L^1(\Omega)}. \tag{9}$$

To speed up the convergence of their algorithm, the authors replaced the total variation of u by its norm in the usual homogeneous Besov space $B_{1,1}^1$ because they just needed to iterate thresholding schemes,

$$\min_{(u,v)} \|u\|_{B_{1,1}^1} + \frac{1}{2\alpha} \|u_0 - u - v\|_{L^2}^2 + \lambda \|v\|_{L^1(\Omega)}. \tag{10}$$

Besides that, Buades et al. [4] observed that value of λ should be chosen as a local indicator so that it takes larger values in textured areas and relatively low values in cartoon regions. To differentiate these regions, they defined a local total variation at each point of the image

$$LTV_{\sigma}(u_0)(x) = (G_{\sigma} * |\nabla u_0|)(x), \tag{11}$$

where G_{σ} is a Gaussian kernel with standard deviation σ . The local indicator λ_{σ} is defined by computing the local total variation of the image around the point, and comparing it to the local total variation after applying a low pass filter to the image

$$\lambda_{\sigma}(x) = \frac{LTV_{\sigma}(u_0)(x) - LTV_{\sigma}(L_{\sigma} * u_0)(x)}{LTV_{\sigma}(u_0)(x)}, \tag{12}$$

with L_{σ} is the low pass filter. If $\lambda_{\sigma}(x) = 0$, this means that the considered point x is taken from a cartoon region. Moreover, when $\lambda_{\sigma}(x) = 1$, the chosen point x belongs to the texture

region. Thus, the authors proposed a nonlinear fast low and high pass filter pair for two-parts decomposition into cartoon and texture, defined as follows:

$$\begin{aligned} u(x) &= w(\lambda_\sigma(x))(L_\sigma * u_0)(x) + (1 - w(\lambda_\sigma(x)))u_0(x), \\ v(x) &= u_0(x) - u(x), \end{aligned}$$

where $w(x) : [0, 1] \rightarrow [0, 1]$ is an increasing function that is constant and equal to zero near zero and close to 1 near 1.

In the above works, the study of minimization problem is made either by using optimization techniques or calculus of variations. However, many researchers proposed to consider a system of partial differential equations instead of one equation. As an example, Elliott et al. [11] proposed a system of two coupled second order equations. Their model results from the H^{-1} gradient flow of the energy consisting of total variation regularization plus the norm H^{-1} of fidelity term. Their model is given as follows:

$$\begin{aligned} \frac{\partial u}{\partial t} - \Delta w &= -\lambda(u - u_0), & \text{in } \Omega_T =]0, T[\times \Omega \\ w &= -\operatorname{div} \left(\frac{Du}{|Du|} \right), & \text{in } \Omega_T, \\ u(0) &= u_0, & \text{in } \Omega, \\ \frac{\partial u}{\partial n} &= \frac{\partial w}{\partial n} = 0, & \text{in } \partial\Omega_T =]0, T[\times \partial\Omega. \end{aligned}$$

A regularization of the function w defined above was suggested by Guo et al. [14]. Their model is given as a reaction diffusion system applied to image restoration and decomposition into cartoon and texture, defined as follows:

$$\begin{aligned} \frac{\partial u}{\partial t} - \operatorname{div} \left(\frac{Du}{|Du|} \right) &= -2\lambda w, & \text{in } \Omega_T, \\ \frac{\partial w}{\partial t} - \Delta w &= -(u_0 - u), & \text{in } \Omega_T, \\ u(0) &= u_0, \quad w(0) = 0, & \text{in } \Omega, \\ \frac{\partial u}{\partial n} &= 0, \quad \frac{\partial w}{\partial n} = 0, & \text{in } \partial\Omega_T, \end{aligned}$$

They proved the following result of existence and uniqueness:

Theorem 1. *If $u_0 \in BV(\Omega)$, then there exists a unique entropy solution (u, w) of the previous system such that:*

$u \in C([0, T]; L^2(\Omega)) \cap L^\infty(0, T; BV(\Omega))$, $\frac{\partial u}{\partial t} \in L^2(Q_T)$, with $u(0, x) = u_0(x)$
 $w \in C([0, T]; L^2(\Omega)) \cap L^\infty(0, T; H^1(\Omega))$, $\frac{\partial w}{\partial t} \in L^2(Q_T)$, with $w(0, x) = 0$,
there exists $z \in L^\infty(Q_T, \mathbb{R}^N)$ with $\|z\|_{L^\infty(Q_T, \mathbb{R}^N)} \leq 1$, $\frac{\partial u}{\partial t} = \operatorname{div}(z) - 2\lambda w$ in Q_T and

$$\int_{\Omega} (u(t) - \varphi) \frac{\partial u}{\partial t} dx \leq \int_{\Omega} z(t) \cdot \nabla \varphi dx - \|Du(t)\| - 2\lambda \int_{\Omega} w(u(t) - \varphi) dx, \quad \text{a.e. on } t \in [0, T]$$

for every $\psi \in C^\infty(\bar{Q}_T)$ with $\psi(x, 0) = \psi(x, T) = 0$,

$$\int_0^T \int_{\Omega} \frac{\partial w}{\partial t} \psi dx dt + \int_0^T \int_{\Omega} \nabla w \cdot \nabla \psi dx dt + \int_0^T \int_{\Omega} (u_0 - u) \psi dx dt = 0$$

This paper is organized as follows: In the next section, we examine the originality of our proposed model. Then, we present the experimental results and discussion respectively in Sections 3 and 4. Finally, we conclude our paper with an opening on some future works.

2 Proposed model

The objective of the proposed method is to modify the model of Osher et al. [19] by considering a new norm of the fidelity term. In fact, in order to extract texture features from the image, we use the norm of the space $L^q(\Omega)$; with $1 < q < 2$ which is weaker than the norm of the L^2 space. To this end, we assume that

$$u_0 - u = \operatorname{div}(\vec{g}),$$

with $\vec{g} \in L^p(\Omega, \mathbb{R}^2)$ (with $1 < p < 2$) is a vector field that admits an L^p -Hodge decomposition. Then, there exists $F \in W_0^{1,p}(\Omega)$ and $\vec{H} \in L^p(\Omega, \mathbb{R}^2)$ such that $\operatorname{div} \vec{H} = 0$ and

$$\vec{g} = \nabla F + \vec{H}. \tag{13}$$

Thus, by applying the divergence operator we have

$$u_0 - u = \operatorname{div}(\vec{g}) = \Delta F. \tag{14}$$

Then, $F = \Delta^{-1}(u_0 - u)$ and we consider the L^p - norm of g instead of L^2 -norm in Osher and al. model. Hence, we obtain the following new convex minimization problem (since $r \mapsto \|r\|^p$ is convex):

$$\min_{u \in BV(\Omega)} \int_{\Omega} |Du| + \frac{\lambda}{p} \int_{\Omega} |\nabla(\Delta)^{-1}(u_0 - u)|^p \tag{15}$$

with $1 < p < 2$. Formally minimizing the energy (15) leads to the Euler-Lagrange equation:

$$-\operatorname{div} \left(\frac{Du}{|Du|} \right) = -\lambda \Delta^{-1}(\operatorname{div}(|\nabla \Delta^{-1}(u_0 - u)|^{p-2} \nabla \Delta^{-1}(u_0 - u))), \tag{16}$$

$$\frac{\partial}{\partial n} \left(\operatorname{div} \left(\frac{Du}{|Du|} \right) \right) = 0, \quad \frac{\partial u}{\partial n} = 0$$

which are partial differential equations of fourth order. Inspired by the ideas of Elliott et al. [11] and Guo et al. [14], we introduce a new model of reaction-diffusion system for image decomposition into cartoon and texture. Precisely, (16) is equivalent to the following two coupled second order equations

$$\begin{aligned} -\operatorname{div} \left(\frac{Du}{|Du|} \right) &= -\lambda v, && \text{in } \Omega, \\ \Delta v &= \operatorname{div}(|\nabla \Delta^{-1} w|^{p-2} \nabla \Delta^{-1} w), && \text{in } \Omega, \\ -\Delta w &= u_0 - u, && \text{in } \Omega, \\ \frac{\partial u}{\partial n} &= 0, \frac{\partial v}{\partial n} = 0, && \text{in } \partial\Omega, \end{aligned}$$

which are the steady state of the following system:

$$u_t - \operatorname{div} \left(\frac{Du}{|Du|} \right) = -\lambda v, \tag{17}$$

$$v_t - \Delta v = \operatorname{div}(|\nabla w|^{p-2} \nabla w), \tag{18}$$

$$w_t - \Delta w = u_0 - u, \tag{19}$$

$$u(0) = u_0, v(0) = 0, w(0) = 0, \tag{20}$$

$$\frac{\partial u}{\partial n} = \frac{\partial v}{\partial n} = \frac{\partial w}{\partial n} = 0, \tag{21}$$

In this model, the function v will contain the oscillating details which is separated from the smooth image u that contains edges and the homogeneous regions of the original image u_0 . The following existence and uniqueness of an entropy solution for the system (22)-(26) is proved by Alaa et al. [26]:

Theorem 2. *If $u_0 \in BV(\Omega)$, then the system (17)-(21) admits one and only one entropy solution (u, v, w) .*

In numerical simulation we add ε to the denominator to avoid dividing by zero in (17)-(21). Then the proposed model is written as follows:

$$u_t - \operatorname{div}((|\nabla u|^2 + \varepsilon)^{\frac{-1}{2}} \nabla u) = -\lambda v, \quad \text{in } \Omega_T, \quad (22)$$

$$v_t - \Delta v = \operatorname{div}((|\nabla w|^2 + \varepsilon)^{\frac{p-2}{2}} \nabla w), \quad \text{in } \Omega_T, \quad (23)$$

$$w_t - \Delta w = u_0 - u, \quad \text{in } \Omega_T, \quad (24)$$

$$u(0) = u_0, v(0) = 0, w(0) = 0, \quad \text{in } \Omega, \quad (25)$$

$$\frac{\partial u}{\partial n} = \frac{\partial v}{\partial n} = \frac{\partial w}{\partial n} = 0, \quad \text{on } \partial\Omega_T. \quad (26)$$

By the way in [26] it is proved that, if $\varepsilon \rightarrow 0$, then the solution $(u_\varepsilon, v_\varepsilon, w_\varepsilon)$ of system (22) - (26) converges to the unique solution of our original system (17) - (21).

3 Numerical Discretization

In general, there are several methods for solving partial differential equations, among others one can refer to [27–32]. However, in image processing as we deal with pixels, finite differences methods and explicit schemes are the most appropriate. In this section, we present a discretization of the proposed model described by (22)-(26). Assuming τ to be the time step size:

$$t = n\tau, \quad n = 0, 1, 2, \dots,$$

$$x = i, \quad 0 \leq i \leq M, y = j, \quad 0 \leq j \leq N ; (x, y) \text{ denote a pixel in a image,}$$

where $M \times N$ is the size of original image. Let's denote by $(u_{i,j}^n, v_{i,j}^n, w_{i,j}^n)$ the approximation of $(u(n\tau, i, j), v(n\tau, i, j), w(n\tau, i, j))$. We define the discrete approximation:

$$\begin{aligned} \nabla_x^+ u_{i,j}^n &= u_{i+1,j}^n - u_{i,j}^n, & \nabla_x^- u_{i,j}^n &= u_{i,j}^n - u_{i-1,j}^n, \\ \nabla_y^+ u_{i,j}^n &= u_{i,j+1}^n - u_{i,j}^n, & \nabla_y^- u_{i,j}^n &= u_{i,j}^n - u_{i,j-1}^n. \end{aligned}$$

We define the discrete approximation of the divergence operator by:

$$\operatorname{div}((|\nabla u^n|^2 + \varepsilon)^{\frac{-1}{2}} \nabla u^n) = \nabla_x^- \left(\frac{\nabla_x^+ u_{i,j}^n}{\sqrt{(\nabla_x^+ u_{i,j}^n)^2 + (\nabla_y^+ u_{i,j}^n)^2 + \varepsilon}} \right) + \nabla_y^- \left(\frac{\nabla_y^+ u_{i,j}^n}{\sqrt{(\nabla_x^+ u_{i,j}^n)^2 + (\nabla_y^+ u_{i,j}^n)^2 + \varepsilon}} \right).$$

The discrete approximation of operator Laplacian for images u^n and v^n is defined by:

$$\begin{aligned} \Delta v_{i,j}^n &= v_{i+1,j}^n + v_{i-1,j}^n + v_{i,j+1}^n + v_{i,j-1}^n - 4v_{i,j}^n, \\ \Delta w_{i,j}^n &= w_{i+1,j}^n + w_{i-1,j}^n + w_{i,j+1}^n + w_{i,j-1}^n - 4w_{i,j}^n. \end{aligned}$$

Then the discrete explicit scheme of our proposed system (22)-(26) can be written as:

$$\begin{aligned}
 u_{i,j}^{n+1} &= u_{i,j}^n + \tau \left[\nabla_x^- \left(\frac{\nabla_x^+ u_{i,j}^n}{\sqrt{(\nabla_x^+ u_{i,j}^n)^2 + (\nabla_y^+ u_{i,j}^n)^2 + \epsilon}} \right) \right] \\
 &\quad + \tau \left[\nabla_y^- \left(\frac{\nabla_y^+ u_{i,j}^n}{\sqrt{(\nabla_x^+ u_{i,j}^n)^2 + (\nabla_y^+ u_{i,j}^n)^2 + \epsilon}} \right) \right] - \tau \lambda v_{i,j}^n, \\
 v_{i,j}^{n+1} &= v_{i,j}^n + \tau \Delta v_{i,j}^n + \tau \left[\nabla_x^- \left(\frac{\nabla_x^+ w_{i,j}^n}{((\nabla_x^+ w_{i,j}^n)^2 + (\nabla_y^+ w_{i,j}^n)^2 + \epsilon)^{\frac{2-p}{2}}} \right) \right] \\
 &\quad + \tau \left[\nabla_y^- \left(\frac{\nabla_y^+ w_{i,j}^n}{((\nabla_x^+ w_{i,j}^n)^2 + (\nabla_y^+ w_{i,j}^n)^2 + \epsilon)^{\frac{2-p}{2}}} \right) \right], \\
 w_{i,j}^{n+1} &= w_{i,j}^n + \tau \Delta w_{i,j}^n + \tau (u_{i,j}^0 - u_{i,j}^n),
 \end{aligned}$$

where

$$\begin{aligned}
 w_{i,j}^0 &= 0, v_{i,j}^0 = 0, u_{i,j}^0 = u_0(ih, jh), \quad 0 \leq i \leq M, 0 \leq j \leq N. \\
 u_{i,0}^n &= u_{i,1}^n, \quad u_{0,j}^n = u_{1,j}^n, \quad u_{M,i}^n = u_{M-1,i}^n, \quad u_{i,N}^n = u_{i,N-1}^n
 \end{aligned}$$

4 Results and discussion

This section is devoted to the numerical experimentations and comparisons. We set the time step size to $\tau = 0.1$ and the parameter p to 1.5. To prove the effectiveness and robustness of the proposed algorithm, a number of experiments is designed and conducted. At first, we show the performance of our model (cf. Figures 1, 2, 3, 5, 7 and 8) in extracting informations from medical images through decomposition process into cartoon and texture components. Then, we establish a comparison with the model of Osher and al. [19] (cf. Figures 1, 2, 3, 6 and 8). Glioblastoma is one of the most aggressive cancer of human brain. The disease manifests itself by headaches, personality changes besides other symptoms. It's very important to detect glioblastoma in its early stages in order to save as many patients as possible. In Figure 1, we consider the decomposition of MRI brain image during different stades of glioblastoma's disease. More precisely, the first column represents the sagittal section of MRI Brain image, the second column illustrates the cartoon component u obtained by Osher and al. model, while the third one contains the cartoon part obtained by the proposed one. Then, the texture images obtained by both models are shown in Figure 2. Let's note that the new model is more efficient in separating the textured details from larger regions: the small textured details are in the texture component, while the homogeneous regions are kept in the cartoon component. In the texture obtained by Osher and al. model, some oscillating details remain on the spinal cord, moreover the cerebellum is still kept in its cartoon component.

In order to make a difference between these details, we display in Figure 3 the contour lines of cartoon component for both models. The cartoon part of Osher and al. model highlights the creation of false edges, around which a large number of contour lines are concentrated. In the

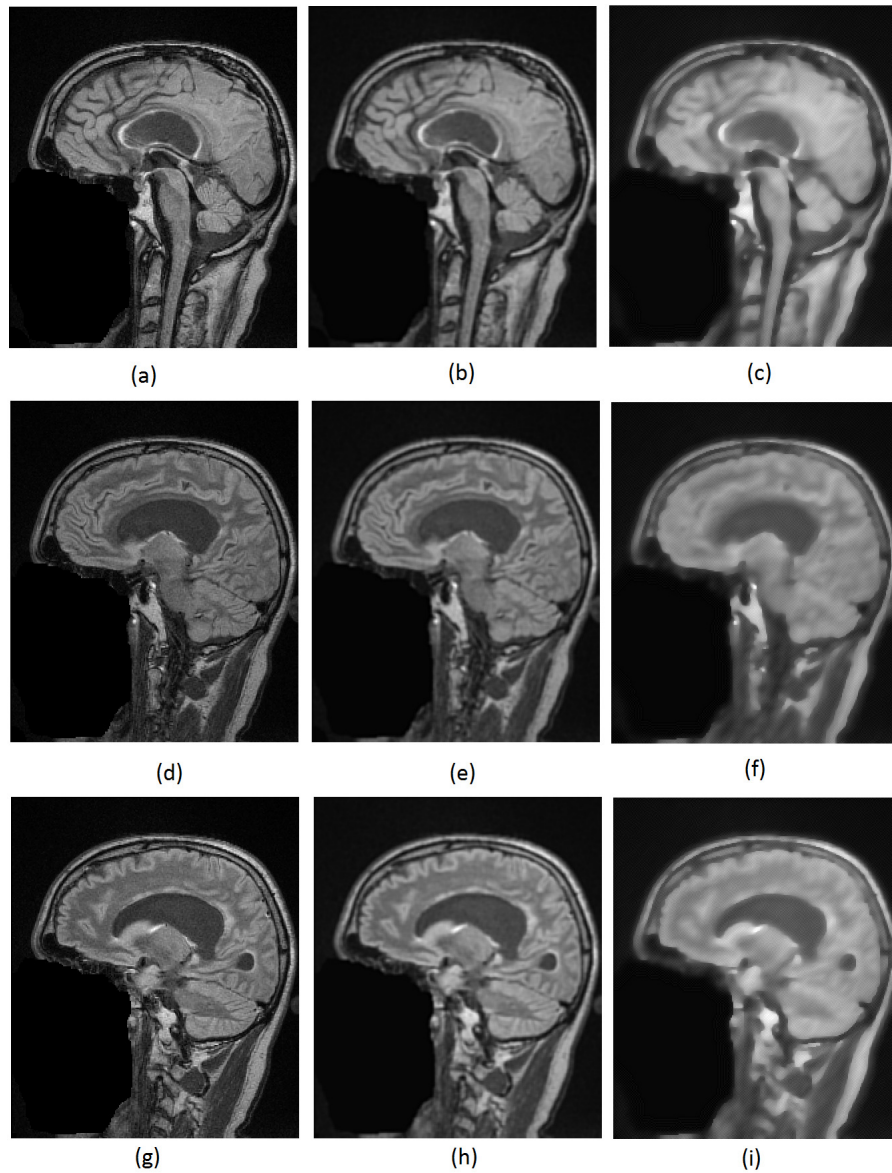


Figure 1: Left: sagittal section of MRI Brain image; Middle: Cartoon part obtained by Osher and al. model; Right: Cartoon part obtained by the proposed model.

contrast, an homogeneous distribution of these lines is remarked in the geometric component obtained by the proposed model. Through this result, we conclude that our method ensure a better decomposition.

In the case of ophthalmic pathologies, diabetic retinopathy is one of the most common complications of diabetes disease, which can attack, silently and for many years, the blood vessels of the retina. Only a regular screening test can diagnose such an abnormality at initial state. In fact, the ophthalmologist notes the observed results on the eye by using an optical

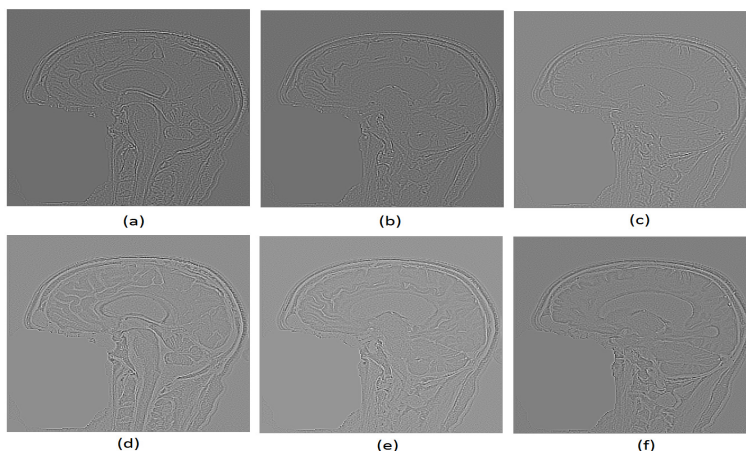


Figure 2: First row: Texture part obtained by Osher and al. model; Second row: Texture part obtained by the proposed model.

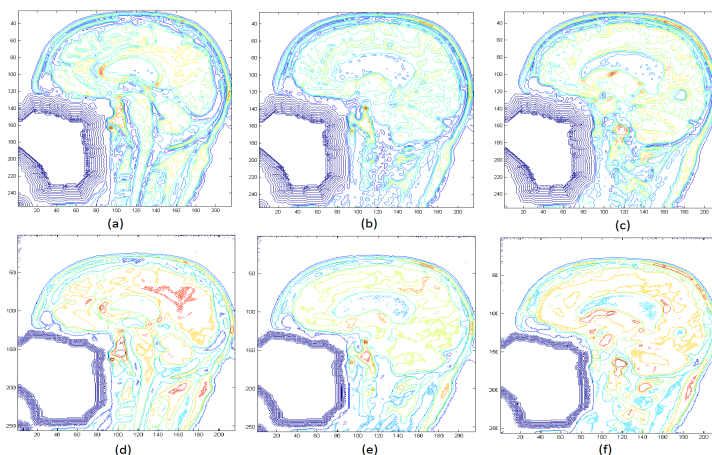


Figure 3: (a), (b) and (c) Contour lines of cartoon part by Osher and al. model; (d), (e) and (f) Contour lines of cartoon part by the proposed model.

camera to see through the eye pupil the rear inner surface of the eyeball. An image is taken showing the optic nerve, the surrounding vessels and the retinal layer. Then, the ophthalmologist can reference this image to prescribe an adequate treatment.

It can be easily understood that such a type of examination varies according to the judgement of the ophthalmologist, and that a great deal of subjectivity persists, especially in case of early onset.

To process these retinal images, several methods have been proposed in the literature. However, it seems that methods using fractal analysis are the most consistent and efficient to give very accurate results. Among these methods, the fractal dimension is one of the parameters used to characterize the complexity of blood vessels. Based on the estimation of this dimension,

one can give a very important interpretation of this measure and consequently have a clear idea about the retina's health.

We have taken a number of pathological retinopathy images from the database DRIVE: (see Figure 4) (<https://www.isi.uu.nl/Research/Databases/DRIVE/>). The evaluation of the

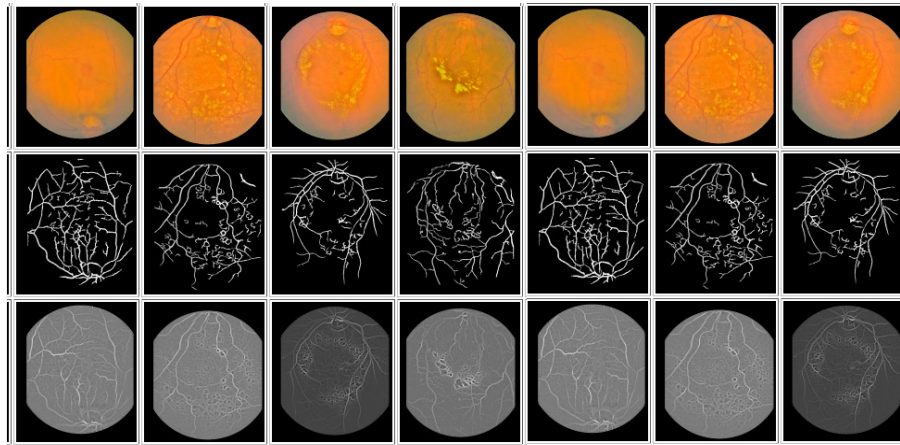


Figure 4: Retinal images.

results is done by comparing the values of fractal dimension (FD) of each abnormal retina with the referential value of FD which equals 1.5 in the case of a normal retina. Let's note that these values are calculated on the texture component of each image by using the "ImageJ method" (<http://imagej.nih.gov/ij/>). The Figure 5 shows the graph of fractal dimension for each pathological case. One can easily notice the broken form of the curve. This variation is due to different degrees of deterioration of retinal blood vessels. The clinical indication of this change is very important because it allows a very precise classification of the alteration stages of the retina.

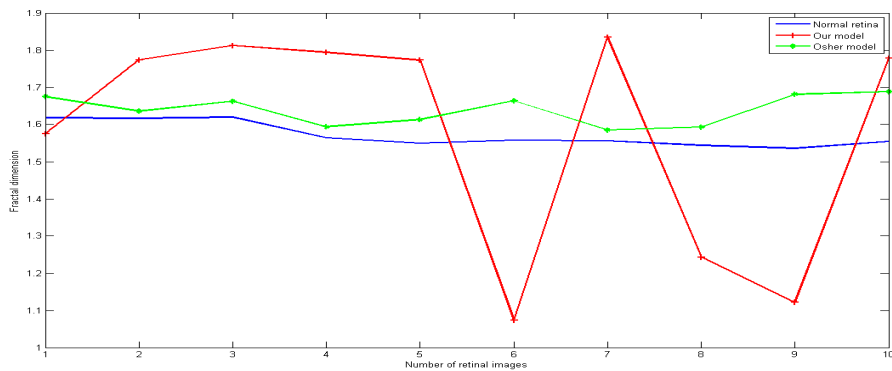


Figure 5: Representation of fractal dimension of each texture retinal image obtained by the proposed model.

In what follows, we illustrate the decomposition of the coronal view of a knee image. In

the first, we show the results obtained by Osher and al. model (see Figure 6) then those of the proposed model (see Figure 7). The texture features are more intensively present in the

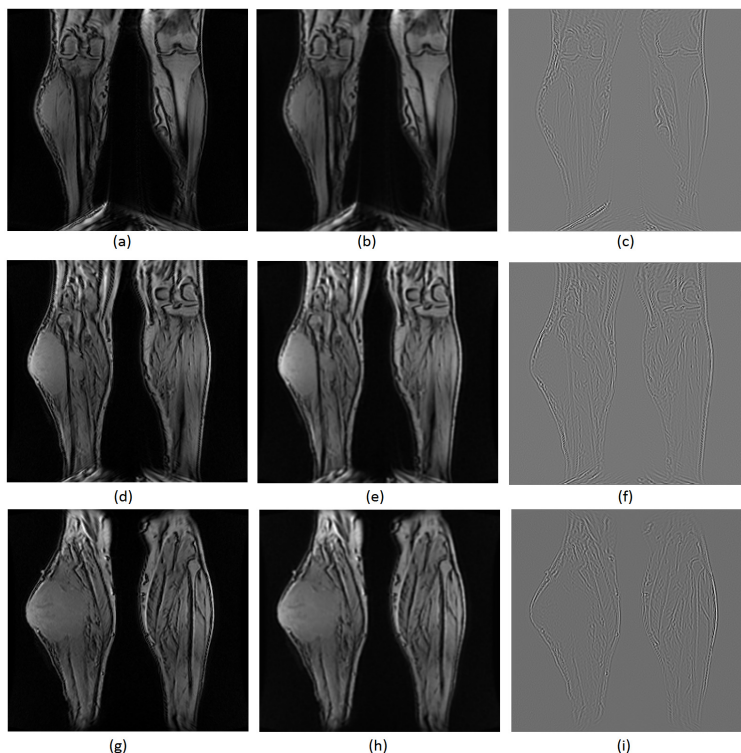


Figure 6: From left to right: original image, cartoon part and texture component obtained by Osher and al. model.

geometric component of Osher and al. model than in the geometric component of the proposed model. To evaluate the difference between both methods, we represent in the next figure (see Figure 8), the profile of line number 100 for both knee image and cartoon component obtained by both models. Precisely, the green curve corresponds to original image whereas the cartoon part of Osher and al. model and the proposed one, are respectively represented by blue and red curves. The smoothness of the proposed model interprets the regular profile shown in the above figure. The small details kept in the cartoon component of the the Osher and al. model, explains why this model follows at the same time the details of the original image.

Finally, we specify that the approximate time to perform each of the simulations on a computing station hp intel(R) Xeon(R) CPU E5-2603 v4 1.70GHz, 6 cores, 6 processors and 20 GB of RAM is of the order of 2 to 5 minutes.

5 Conclusion

The proposed system obtained from the modification of Osher and al. model, gives better results in separating biomedical images into two well-defined components. Precisely, the new method is

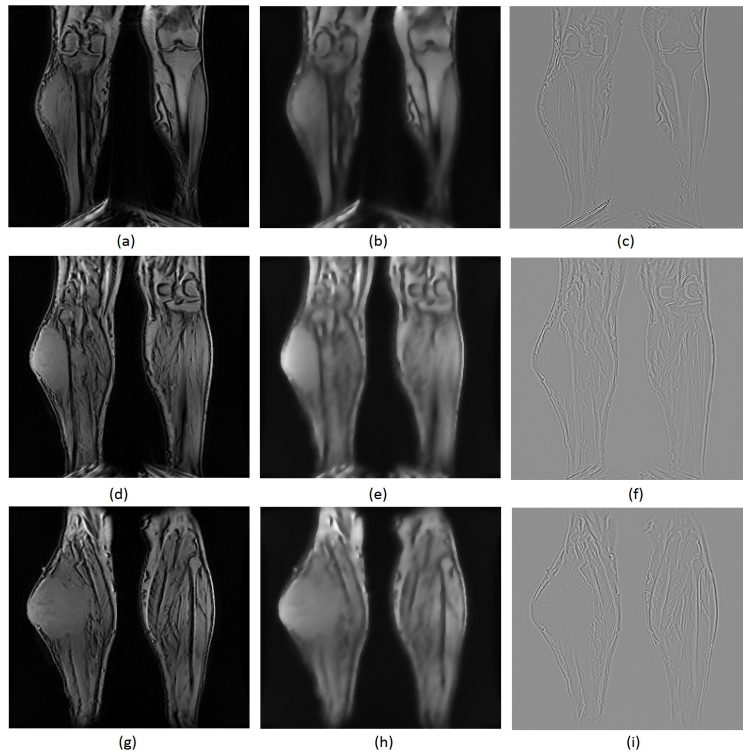


Figure 7: From left to right: original image, cartoon part and texture component obtained by proposed model.

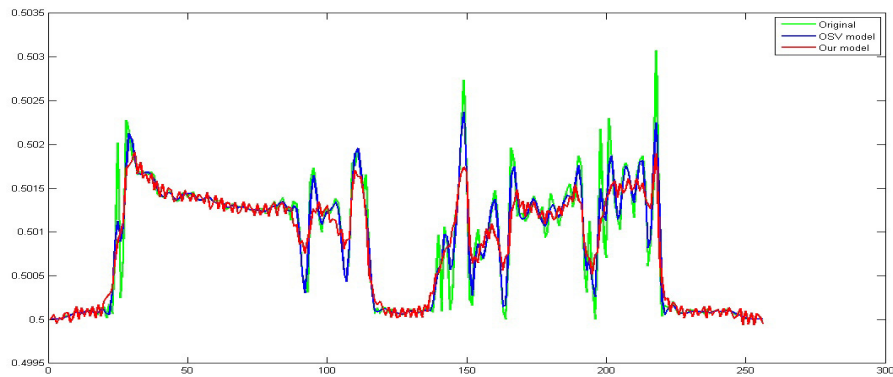


Figure 8: Line profile number 100 of original, cartoon images for both models.

more appropriate to keep the homogeneous regions and boundaries in the geometric component and to represent textured or oscillatory patterns. In the future work, we will prove the existence and uniqueness of solution for our system.

Appendix

All data from human patients were anonymized in consideration of the protection of their intellectual properties, and were free available to browse, download, and use for commercial, scientific and educational purposes at the RIDER Neuro MRI and TCGA-SARC collections in The Cancer Imaging Archive TCIA (<http://www.cancerimagingarchive.net/>).

Data Citation: Barboriak, Daniel. (2015). Data From RIDER_NEURO_MRI. The Cancer Imaging Archive. <http://doi.org/10.7937/K9/TCIA.2015.VOSN3HN1>.

TCIA Citation: [9].

TCGA Attribution: The results published or shown here are in whole or part based upon data generated by the TCGA Research Network: <http://cancergenome.nih.gov/>.

Data Citation: Roche, C., Bonaccio, E., Filippini, J. (2016). Radiology Data from The Cancer Genome Atlas Sarcoma [TCGA-SARC] collection. The Cancer Imaging Archive. <http://doi.org/10.7937/K9/TCIA.2016.CX6YLSUX>.

TCIA Citation: [9]. The retinal images are available at the database DRIVE: (<https://www.isi.uu.nl/Research/Databases/DRIVE/>).

Publication Citation: [22].

References

- [1] J.F. Aujol, G. Gilbao, *Implementation and parameter selection for BV-Hilbert space regularizations*, UCLA CAM Report (2004) 1–46.
- [2] J.F. Aujol, G. Gilbao, T. Chan, S. Osher, *Structure-texture image decomposition-modeling, algorithms, and parameter selection*, Int. J. Comput. Vis. **67** (2006) 111–136.
- [3] M. Brady, S. Petroudi, *Classification of Mammographic Texture Patterns*, Proc 7th Int Workshop of Digital Mammography, Chapel Hill, NC, USA, 2004.
- [4] A. Buades, T.M. Le, J.M. Morel, L.A. Vese, *Fast cartoon + texture image filters*, IEEE Trans. Image Process. **19** (2010) 1978–1986.
- [5] F. Chabat, D.M. Hansell, G.Z. Yang, *Obstructive lung diseases: texture classification for differentiation at CT*, Radiology **228** (2003) 871–877.
- [6] A. Chambolle, *An algorithm for total variation minimization and applications*, J. Math. Imaging Vis. **20** (2004) 89–97.
- [7] A. Chambolle, P.L. Lions, *Image recovery via total variation minimization and related problems*, Numer. Math. **76** (1997) 167–188.
- [8] A. Chambolle, T. Pock, *A first-order primal-dual algorithm for convex problems with applications to imaging*, J. Math. Imaging. Vis. **40** (2011) 120–145.

- [9] K. Clark, B. Vendt, K. Smith, J. Freymann, J. Kirby, P. Koppel, S. Moore, S. Phillips, D. Maffitt, M. Pringle, L. Tarbox, F. Prior, *The Cancer Imaging Archive (TCIA): Maintaining and Operating a Public Information Repository*, J. Digit. Imaging **26** (2013) 1045–1057.
- [10] T.M. Deserno, *Biological and Medical Physics, Biomedical Engineering*, Springer, Verlag Berlin Heidelberg, 2010.
- [11] J.C.M. Elliott, S. A. Smitheman, *Analysis of the TV regularization and H^{-1} fidelity model for decomposing an image into cartoon plus texture*, Commun. Pure Appl. Anal. **6** (2007) 917–936.
- [12] Y. Tao, S.-C.B. Lo, M.T. Freedman, E. Makariou, J. Xuan, *Automatic categorization of mammographic masses using BI-RADS as a guidance*, Proc. SPIE 6915, Medical Imaging 2008: Computer-Aided Diagnosis, 691526, 2008.
- [13] M. Ghoneim, G. Toussaint, J. M. Constants, *Three dimensional texture analysis in MRI: a preliminary evaluation in gliomas*, Magn. Reson. Imaging **21** (2003) 983–987.
- [14] Z. Guo, J. Yin, Q. Liu, *On a reaction-diffusion system applied to image decomposition and restoration*, Math. Comput. Model. **53** (2011) 1336–1350.
- [15] V.A. Kovalev, M. Petrou, J. Suckling, *Detection of structural differences between the brains of schizophrenic patients and controls*, Psychiatry Res. **124** (2003) 177–189.
- [16] Y. Meyer, *Oscillating Patterns in Image Processing and Nonlinear Evolution Equations*, in: Univ. Lecture Ser., AMS, Providence, RI, 2002.
- [17] M.S. Neofytou, T. Vasilis, M.S. Pattichis, *A standardised protocol for texture feature analysis of endoscopic images in gynaecological cancer*, Biomed. Eng. Online **29** (2007) 6–44.
- [18] T. Kalaiselvi, S. Karthiagi Selvi, *Energy update restricted ChanVese model for tumor extraction from MRI of human head scans*, Int. J. Comput. Methods **15** (2018) 1750081.
- [19] S. Osher, A. Solé, L. Vese, *Image decomposition and restoration using total variation minimization and the H^{-1} norm*, SIAM J. Multiscale Model. **1** (2003) 349–370.
- [20] L. Rudin, S. Osher, E. Fatemi, *Nonlinear total variation based noise removal algorithms*, Physica. D. **60** (1992) 259–268.
- [21] A. Sayeed, M. Petrou, N. Spyrou, *Diagnostic features of Alzheimer’s disease extracted from PET sinograms*, Phys. Med. Biol. **47** (2002) 137–148.
- [22] J.J. Staal, M.D. Abramoff, M. Niemeijer, M.A. Viergever, B. van Ginneken, *Ridge based vessel segmentation in color images of the retina*, IEEE Trans. Med. Imaging **23** (2004) 501–509.
- [23] V.L. Guen, *Cartoon + texture image decomposition by the TV-L1 model*, Image Processing On Line **4** (2014) 204–219.

- [24] T.J. Dennis, N. G. Dessipris, *Fractal modelling in image texture analysis*, IEE Proceedings F (Radar and Signal Processing) **136** (1989) 227–235.
- [25] A. Heshmati, M. Gholami, A. Rashno, *Scheme for unsupervised colour texture image segmentation using neutrosophic set and non-sampled contourlet transform*, IET Image Process. **10** (2016) 21–43.
- [26] M. Zirhem, N. E. Alaa, *Existence and uniqueness of an entropy solution for a nonlinear reaction-diffusion system applied to texture analysis*, J. Math. Anal. Appl. **484** (2020) 123719.
- [27] M. Ilati, *Analysis and application of the interpolating element-free Galerkin method for extended Fisher-Kolmogorov equation which arises in brain tumor dynamics modeling*, Numer. Algorithms **85** (2020) 485–502.
- [28] M. Ilati, M. Dehghan, *Meshless local weak form method based on a combined basis function for numerical investigation of Brusselator model and spike dynamics in the Gierer-Meinhardt system*, Comput. Model. Eng. Sci. **109** (2015) 325–360.
- [29] M. Ilati, M. Dehghan, *Application of direct meshless local Petrov-Galerkin (DMLPG) method for some Turing type models*, Eng. Comput. **33** (2017) 107–124.
- [30] M. Ilati, M. Dehghan, *Remediation of contaminated groundwater by meshless local weak forms*, Comput. Math. Appl. **72** (2016) 2408–2416.
- [31] M. Dehghan, M. Abbaszadeh, *Numerical study of three-dimensional Turing patterns using a meshless method based on moving Kriging element free Galerkin (EFG) approach*, Comput. Math. Appl. **72** (2016) 427–454.
- [32] M. Abbaszadeh, M. Dehghan, *A reduced order finite difference method for solving space-fractional reaction-diffusion systems: The Gray-Scott model*, Eur. Phys. J. Plus **134** (2019) 620.